

Self-learning Monte Carlo method with Behler–Parrinello neural networks

Yuki Nagai,^{1,2} Masahiko Okumura,¹ and Akinori Tanaka^{2,3,4}

¹*CCSE, Japan Atomic Energy Agency, 178-4-4, Wakashiba, Kashiwa, Chiba, 277-0871, Japan*

²*Mathematical Science Team, RIKEN Center for Advanced Intelligence Project (AIP),
1-4-1 Nihonbashi, Chuo-ku, Tokyo 103-0027, Japan*

³*Department of Mathematics, Faculty of Science and Technology,
Keio University, 3-14-1 Hiyoshi, Kouhoku-ku, Yokohama 223-8522, Japan*

⁴*interdisciplinary Theoretical & Mathematical Sciences Program
(iTHEMS) RIKEN 2-1, Hirosawa, Wako, Saitama 351-0198, Japan*

(Dated: December 4, 2021)

We propose a general way to construct an effective Hamiltonian in the Self-learning Monte Carlo method (SLMC) method, which speeds up Monte Carlo simulations by training an effective model to propose uncorrelated configurations in the Markov chain. Its applications are, however, limited. This is because it is not obvious to find the explicit form of the effective Hamiltonians. Particularly, it is difficult to make effective Hamiltonians including many body interactions. In order to overcome this critical difficulty, we introduce the Behler–Parrinello neural networks (BPNNs) as “effective Hamiltonian” without any prior knowledge, which is used to construct the potential-energy surfaces in interacting many particle systems for molecular dynamics. We construct self-learning continuous-time interaction-expansion quantum Monte Carlo method with BPNNs and apply it to quantum impurity models. We observed significant improvement of the acceptance ratio from 0.01 (the effective Hamiltonian with the explicit form) to 0.76 (BPNN). This drastic improvement implies that the BPNN effective Hamiltonian includes many body interaction, which is omitted in the effective Hamiltonian with the explicit forms. The BPNNs make SLMC more promising.

I. INTRODUCTION

Quantum Monte Carlo (QMC) is one of the unbiased numerical methods for studying quantum many-body systems^{7–10}. The developments of the continuous-time QMC have made great successes for strongly correlated electron systems^{11–14}. In this algorithm, the partition function is expanded in the powers of the perturbation terms. Both the number and position of perturbation terms on the imaginary-time interval change constantly during the simulation. To compute the weight of each configuration, the continuous-time QMC methods require integrating out the fermions, which is very time consuming.

The self-learning Monte Carlo (SLMC)^{15,17,18,22} was recently introduced as a general method, which speeds up the MC simulation by designing and training a model to propose efficient global updates. There are many kinds of applications, such as classical statistical mechanics models^{15,16}, classical spin-fermion models¹⁷, determinant QMC^{18–20}, continuous-time QMC^{21,22}, and hybrid MC in high-energy physics²³. The SLMC is one of the successes in machine learning techniques in physics^{24–30,32–39}. The philosophy behind SLMC is “first learn, then earn”. In the learning stage, we perform trial simulations to generate a large set of configurations and their weights. These configurations and weights are then used to train an effective model H_{eff} , whose Boltzmann weight $e^{-\beta H_{\text{eff}}}$ fits the probability distribution of the original problem. Next, in the actual simulation, H_{eff} is used as a guide to propose highly efficient global moves in configuration space.

A good effective model makes simulations with the SLMC more efficient. The efficient effective model is

usually invented based on the human understanding of the original system^{15,17–19,22}. However, it is not easy to construct effective models including many body interaction, since we do not know systematic procedure applicable in arbitrary systems. Recently, H. Shen *et al.* gave pioneering work to construct the effective Hamiltonian including many body interaction without explicit forms using the convolutional deep neural network (CNN)⁴⁰. Although the CNN method is powerful, its applicability is limited to the system whose particle configurations are given by discrete indices. This is because the inputs of the CNN is usually discretized like pixels in a digital picture. For example, SLMC with the CNN cannot be applied to the continuous-time QMC, since the inputs of the continuous-time QMC have both discrete position on a lattice and continuous imaginary-time. Therefore, further extension of SLMC with neural networks are needed.

The machine learning including artificial neural networks have been used for about twenty years in the field of the molecular dynamics (MD) to construct the potential-energy surfaces (PESs) providing inter-atom forces with accuracy and computational complexity respectively comparable to quantum and classical mechanical calculations. In the method, the neural network is trained using a large data set consisting of pairs of an atom configuration with continuous position index and corresponding total energy in some systems given by quantum mechanical calculation (e.g., the density functional theory)⁴⁴. We point out that the neural network PESs can be considered as a general scheme to construct effective Hamiltonians of systems consisting of interacting particles with continuous indices. The wide applicability of this method allow us to apply it to complex

problems like the imaginary-time MC calculation of electrons in a solid, which has both discrete and continuous coordinates corresponding to positions on a lattice and imaginary-time, respectively.

In this paper, we propose a method to construct the effective Hamiltonians with Behler–Parrinello neural networks (BPNN)⁴⁴, which is one of most succeeded methods in the field of the molecular dynamics with machine learning. We regard the the configuration and effective Hamiltonian in SLMC as the positions of the atoms and the PESs in the MD, respectively. We use the recently proposed method⁴⁶ to map continuous coordinates (atom positions) onto discrete (inputs of BPNN) variables, whose advantage is availability of systematic improvement of the mapping accuracy. As a concrete example, we demonstrate self-learning continuous-time interaction-expansion (CTINT) QMC with BPNNs on quantum impurity models. We implement the simplest neural networks and test their performances. We also develop the fast updates which is applicable even with deep neural networks to reduce the computational cost significantly in the SLMC simulation.

The paper is organized as follows. The Markov chain Monte Carlo method is briefly described in Sec.II, the self-learning Monte Carlo method is introduced in Sec. III, The Machine-learning technique in molecular dynamics and Behler–Parrinello neural networks are introduced in Sec.IV, the SLMC and BPNN is combined in Sec.V, the SLMC on quantum impurity models is demonstrated in Sec. VI, the discussion is given in Sec. VII, and the conclusion is given in Sec.VIII.

II. MARKOV PROCESS MONTE CARLO METHOD IN PHYSICS

The Markov process Monte Carlo method (MCMC) is a powerful method for an integration in high-dimensional space. Partition functions and physical exception values are calculated by the MCMC. We describe the MCMC method in Physics and point out its problems and difficulties in the following.

A. Multi-dimensional integration

Let us consider the following multi-dimensional integration:

$$I = \int \cdots \int dx_1 \cdots dx_N w(x_1, \cdots, x_N) f(x_1, \cdots, x_N), \quad (1)$$

where $w(x_1, \cdots, x_N)$ is a localized function in N -dimensional space, and $f(x_1, \cdots, x_N)$ is an arbitral function. In the Monte Carlo method, the integration I is

approximated as

$$I \sim \sum_{\mathcal{C}} f(x_1, \cdots, x_N), \quad (2)$$

where $\mathcal{C} = (x_1, \cdots, x_N)$ is randomly generated with the probability $w(x_1, \cdots, x_N)$, which is called a configuration.

In Physics, the partition function Z and physical exception value $\langle A \rangle$ are expressed with the multi-dimensional integration:

$$Z = \int \cdots \int d\phi_1 \cdots d\phi_N e^{-S(\phi_1, \cdots, \phi_N)}, \quad (3)$$

$$\langle A \rangle = \frac{1}{Z} \int \cdots \int d\phi_1 \cdots d\phi_N A(\phi_1, \cdots, \phi_N) e^{-S(\phi_1, \cdots, \phi_N)}. \quad (4)$$

For example, the physical exception value $\langle A \rangle$ in the classical Ising model on one-dimensional lattice is expressed as

$$\langle A \rangle = \frac{1}{Z} \sum_{s_1, \cdots, s_N} A(s_1, \cdots, s_N) e^{-\beta E(s_1, \cdots, s_N)}, \quad (5)$$

$$\sim \frac{1}{Z} \sum_{\mathcal{C}} A(s_1, \cdots, s_N). \quad (6)$$

where $Z = \sum_{s_1, \cdots, s_N} \exp(-\beta E(s_1, \cdots, s_N))$, β is an inverse temperature, N is a number of spins, $s_i = \pm 1$, $E(s_1, \cdots, s_N) = J \sum_{\langle i, j \rangle} s_i s_j$, and $\sum_{\langle i, j \rangle}$ is a summation of the nearest neighbor spins. The configuration $\mathcal{C} = (s_1, \cdots, s_N)$ is randomly generated with the Boltzmann weight $e^{-\beta E(s_1, \cdots, s_N)}$.

B. Metropolis-Hastings algorithm

In the Monte Carlo method, we have to generate the configuration \mathcal{C} with the probability distribution $w(\mathcal{C})$. By constructing a Markov chain that has the desired distribution as its equilibrium distribution, we can obtain a sample of the desired distribution by observing the chain after a number of steps. To construct the Markov chain, we introduce the condition of the detailed balance expressed as

$$w(\mathcal{C})P(\mathcal{C}'|\mathcal{C}) = w(\mathcal{C}')P(\mathcal{C}|\mathcal{C}'). \quad (7)$$

Here, $P(\mathcal{C}'|\mathcal{C})$ is the probability of transitioning from a configuration \mathcal{C} to a configuration \mathcal{C}' . The Metropolis-Hastings approach is to separate the transition in two sub-steps:

$$P(\mathcal{C}'|\mathcal{C}) = g(\mathcal{C}'|\mathcal{C})A(\mathcal{C}', \mathcal{C}), \quad (8)$$

where the proposal distribution $g(\mathcal{C}'|\mathcal{C})$ is the conditional probability of proposing a configuration \mathcal{C}' given \mathcal{C} , and the acceptance ratio $A(\mathcal{C}', \mathcal{C})$ is the probability to accept

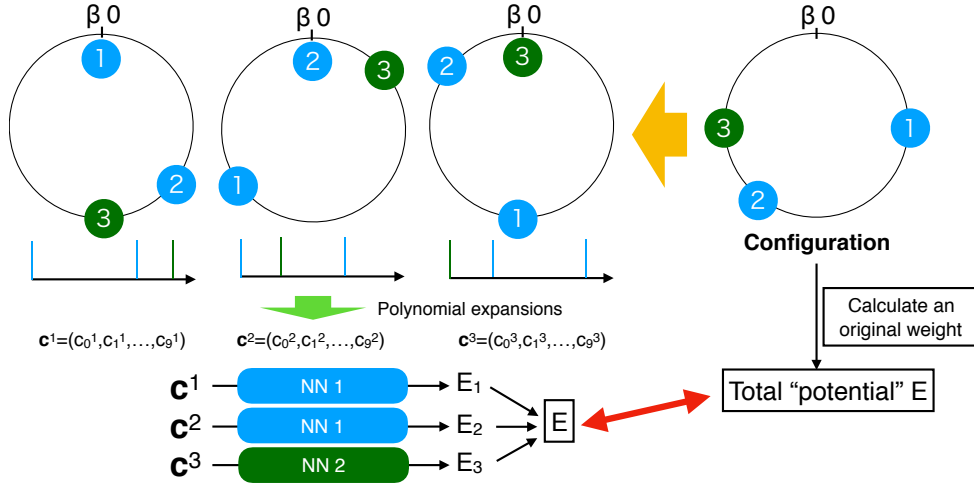


FIG. 1. (Color online) Schematic figures of Behler-Parrinello neural networks for the self-learning continuous-time interaction-expansion quantum Monte Carlo method. The configuration with N vertices on the imaginary-time axis $\mathcal{C} = \{\tau_1, \tau_2, \dots, \tau_N\}$ is mapped to the set of the “element-wise” configurations $\mathcal{C}^{\text{ele}}(\tau_i - \tau_j)$ around a vertex j : $\mathcal{C} \rightarrow \{\mathcal{C}^{\text{ele}}(\tau_1 - \tau_j), \mathcal{C}^{\text{ele}}(\tau_2 - \tau_j), \dots, \mathcal{C}^{\text{ele}}(\tau_N - \tau_j)\}$. The element-wise configuration is expressed as a distribution function with δ functions. The total potential E of the original calculation is expressed as $E = \log w(\mathcal{C})/(-\beta)$. E obtained by the neural networks is expressed as $E = \log w^{\text{eff}}(\mathcal{C})/(-\beta) = H_{\text{eff}}(\mathcal{C})$. The partial energy E_i is defined as $E_i = h_{\text{eff}}^{\alpha_i}(\mathbf{c}^j)/(-\beta)$. The color of the circle denotes a kind of a vertex. Same neural networks are used if the kind of a vertex is same.

the proposed configuration \mathcal{C}' . By inserting the above expression into Eq. (7), we have

$$\frac{A(\mathcal{C}', \mathcal{C})}{A(\mathcal{C}, \mathcal{C}')} = \frac{w(\mathcal{C}') g(\mathcal{C}|\mathcal{C}')}{w(\mathcal{C}) g(\mathcal{C}'|\mathcal{C})}. \quad (9)$$

The Markov chain that has the desired distribution $w(\mathcal{C})$ is obtained when the acceptance ratio is given as

$$A(\mathcal{C}', \mathcal{C}) = \min \left(1, \frac{w(\mathcal{C}') g(\mathcal{C}|\mathcal{C}')}{w(\mathcal{C}) g(\mathcal{C}'|\mathcal{C})} \right). \quad (10)$$

Then, we can generate the Markov chain expressed as

$$\mathcal{C}_1 \rightarrow \dots \rightarrow \mathcal{C}_i \rightarrow \dots. \quad (11)$$

C. Design of the proposals

One can design various kinds of the Monte Carlo method based on Eq. (10). We need the update method from \mathcal{C} to \mathcal{C}' with the high acceptance ratio for good efficiency of the MCMC.

1. Hand-designed proposals: conventional local and global updates

The most simple update method is so-called local update, where the configuration is updated locally. One randomly chooses a single site in the current configuration and proposes a new configuration by changing the variable on this site. For example, in the Ising spin

model, the candidate of the next configuration is generated by flipping a randomly chosen spin. In this case, the proposal probability $g(\mathcal{C}'|\mathcal{C})$ from \mathcal{C}' to \mathcal{C} equals $g(\mathcal{C}|\mathcal{C}')$ from \mathcal{C} to \mathcal{C}' . The acceptance ratio in Eq. (10) becomes $A(\mathcal{C}', \mathcal{C}) = \min \left(1, \frac{w(\mathcal{C}')}{w(\mathcal{C})} \right)$. In the local update, one can expect that $w(\mathcal{C})$ is similar to $w(\mathcal{C}')$ so that the acceptance rate is high, since the configuration \mathcal{C} is similar to \mathcal{C}' . Although the local update is general-purpose, model-independent method, there is an evident disadvantage. When $w(\mathcal{C}')$ is not similar to $w(\mathcal{C})$ even if \mathcal{C}' is similar to \mathcal{C} , it is hard to obtain uncorrelated configurations. Thus, the local update suffers heavily from a critical slowing down close to phase transitions. In such cases, the autocorrelation time within the Markov chain τ becomes very large.

To overcome the increase of the autocorrelation time for the local update, various kinds of global update method have been developed¹⁻⁵. In all these global update methods, variables on a large number of sites are simultaneously changed in a single Monte Carlo update. The autocorrelation time τ can be reduced in these methods. The global update method is designed for specific model, since one has to use properties that a model has to obtain good efficiency. For example, the Wolff method can simulate the two-dimensional Ising model. However, by adding the interaction among the four spins in the same plaquette to this model, no simple and efficient global update method is known¹⁵. For a given generic model, it is hard to design an efficient global update method.

2. Proposals by time evolution: Hybrid Monte Carlo updates

The hybrid Monte Carlo (HMC) method is known as the one of the good global update methods, which is widely used in the lattice quantum chromodynamics (QCD). In the HMC, by introducing pseudo momentum, the pseudo-time evolution from the configuration \mathcal{C} , which is called a molecular dynamics (MD) evolution in analogy to simulations of classical particles, generates the next configuration \mathcal{C}' . In this method, the proposal probability $g(\mathcal{C}|\mathcal{C}')$ from \mathcal{C}' to \mathcal{C} equals $g(\mathcal{C}'|\mathcal{C})$ from \mathcal{C} to \mathcal{C}' , since the time evolution due to the Hamiltonian dynamics is time-reversal symmetric. The exact MD evolution due to the Hamilton equation conserves "energy" $\log w$. In actual simulation, the discretized time step changes the energy. Thus, the MD evolution generates the configuration \mathcal{C}' whose probability $w(\mathcal{C}')$ is similar to $w(\mathcal{C})$ so that the acceptance ratio $A(\mathcal{C}', \mathcal{C}) = \min\left(1, \frac{w(\mathcal{C}')}{w(\mathcal{C})}\right)$ is high. Recently, the HMC method is revisited in the condensed matter physics to treat strongly correlated electron systems⁶, since the HMC method is general to obtain uncorrelated configurations. Although the HMC method might be suitable for reducing the autocorrelation time, its computational cost of the HMC is not small. One has to calculate the forces which is the derivative of the energy to do the MD evolution. For example, in the lattice QCD simulation, the inverse matrices related to the Dirac operator on four dimensional lattice have to be calculated.

III. SELF-LEARNING MONTE CARLO METHOD

A. Basic concept

In the MCMC, we can design the proposal probability $g(\mathcal{C}|\mathcal{C}')$. If the ratio of the probability $g(\mathcal{C}|\mathcal{C}')/g(\mathcal{C}'|\mathcal{C}) = w(\mathcal{C})/w(\mathcal{C}')$, the new configuration \mathcal{C}' is always accepted (i.e. $A(\mathcal{C}', \mathcal{C}) = 1$). To design the proposal probability, we use the another Markov chain with the probability $w_{\text{prop}}(\mathcal{C})$. We consider that the configuration \mathcal{C}' is obtained by the random walk from \mathcal{C} on this proposal Markov chain. Its detailed balance condition is given as

$$w_{\text{prop}}(\mathcal{C})P_{\text{prop}}(\mathcal{C}'|\mathcal{C}) = w_{\text{prop}}(\mathcal{C}')P_{\text{prop}}(\mathcal{C}|\mathcal{C}'). \quad (12)$$

This proposal probability $P_{\text{prop}}(\mathcal{C}'|\mathcal{C})$ can be regarded as the conditional probability $g(\mathcal{C}'|\mathcal{C})$ on the original Markov chain, which proposes a configuration \mathcal{C}' from given \mathcal{C} . Thus, with the use of the relation:

$$\frac{g(\mathcal{C}|\mathcal{C}')}{g(\mathcal{C}'|\mathcal{C})} = \frac{w_{\text{prop}}(\mathcal{C})}{w_{\text{prop}}(\mathcal{C}')}, \quad (13)$$

the acceptance ratio in the SLMC is given as

$$A(\mathcal{C}', \mathcal{C}) = \min\left(1, \frac{w(\mathcal{C}')}{w(\mathcal{C})} \frac{w_{\text{prop}}(\mathcal{C})}{w_{\text{prop}}(\mathcal{C}')}\right). \quad (14)$$

TABLE I. Difference between three update methods

	Hand-designed	HMC	SLMC
Propose method	by hand	MD	Markov chain
$g(\mathcal{C} \mathcal{C}')/g(\mathcal{C}' \mathcal{C})$	usually 1	1	$w_{\text{eff}}(\mathcal{C})/w_{\text{eff}}(\mathcal{C}')$

If we can design the proposal Markov chain whose probability is equal to that of the original Markov chain $w_{\text{prop}}(\mathcal{C}) = w(\mathcal{C})$, the proposed configuration \mathcal{C}' is always accepted. The average acceptance rate $\langle A \rangle$ can be estimated by $\langle A \rangle = \exp\left[-\sqrt{\text{MSE}}\right]$ with the mean squared error $\text{MSE} = (1/n) \sum_i (\ln w_{\text{prop}}(\mathcal{C}_i) - \ln w(\mathcal{C}_i))^2$.⁴⁰ Here, n is the number of the measurements in Monte Carlo simulations.

The difference between several update methods is shown in Table I. The HMC and SLMC are global updates where the configurations are changed globally. In the SLMC, the configuration is proposed by the proposal Markov chain. We have to find a good proposal Markov chain whose probability $w_{\text{prop}}(\mathcal{C})$ is similar to original one $w(\mathcal{C})$.

To design the proposal Markov chain, we have to construct an effective model. We introduce an effective Hamiltonian $H_{\text{eff}}(\mathcal{C})$:

$$w_{\text{prop}}(\mathcal{C}) = w^{\text{eff}}(\mathcal{C}) = \exp[-\beta H_{\text{eff}}(\mathcal{C})]. \quad (15)$$

This model $H_{\text{eff}}(\mathcal{C})$ can be constructed by a supervised machine-learning technique¹⁵. In the learning stage, trial simulations are performed to generate a large set of configurations and their weights. These data are then used to train an effective model $H_{\text{eff}}(\mathcal{C})$, whose weight fits the probability distribution of the original problem $w(\mathcal{C})$. Next, in the actual simulation, $H_{\text{eff}}(\mathcal{C})$ is used as a guide to propose highly efficient global moves in configuration space. It is important to obtain good effective models in the SLMC simulations. In the previous study²², we have successfully obtained the form of the effective Hamiltonian with two-body interactions in the continuous-time auxiliary-field QMC (CTAUX) for the Anderson impurity model. In the CTINT simulations, Huang *et al.* have produced the classical Hamiltonian with two- and three-body interactions to reproduce the weights²¹. However, it seems hard to construct the effective Hamiltonian in other systems or other methods.

B. Autocorrelation time of the SLMC

We show that the autocorrelation time of the SLMC can be estimated by the average acceptance ratio $\langle A \rangle$. We consider the autocorrelation time of the original MC simulation τ_{original} and that of the SLMC τ_{SLMC} . If the effective Hamiltonian is perfect $w^{\text{eff}}(\mathcal{C}) = w(\mathcal{C})$, the average acceptance ratio is always one $\langle A \rangle = 1$. In this case, if the length of the proposal Markov chain is longer

TABLE II. Similarity between first-principle-based MD and QMC

	MD	QMC
Input	atomic positions	configurations
Time-consuming	DFT calculation	weight calculation
Output	potential energy	weight

than τ_{original} , there is no correlation between the previous and proposed configurations \mathcal{C} and \mathcal{C}' . Thus, the autocorrelation time of the SLMC τ_{SLMC} should be one. When the autocorrelation time of the original MC simulation τ_{original} is long, we can use more longer proposal Markov chain to obtain uncorrelated configurations. If the effective Hamiltonian is not perfect, the proposal configuration is accepted by the acceptance ratio $\langle A \rangle$. Even in this case, we can choose the length of the proposal Markov chain to obtain uncorrelated configurations. Thus, the autocorrelation time of the SLMC τ_{SLMC} should be $\tau_{\text{SLMC}} \sim 1/\langle A \rangle$. In general, the autocorrelation time τ_{SLMC} is expressed as

$$\tau_{\text{SLMC}} \sim \min \left(1, \frac{\tau_{\text{original}}}{N_{\text{steps}}^{\text{prop}}} \right) \frac{1}{\langle A \rangle}, \quad (16)$$

where $N_{\text{steps}}^{\text{prop}}$ is the length of the proposal Markov chain.

C. Effective two-body interaction

The problem in SLMC is how to construct effective Hamiltonian $\ln w^{\text{eff}}(\mathcal{C})$ to fit the Hamiltonian $\ln w(\mathcal{C})$ as a functional of \mathcal{C} . The most simplest effective Hamiltonian has two-body interactions defined as

$$H_{\text{eff}}(\mathcal{C}) = \sum_{ij}^M L(\mathcal{C}_i, \mathcal{C}_j), \quad (17)$$

where \mathcal{C}_i is the i -th element of the configuration $\mathcal{C} = (\mathcal{C}_1, \dots, \mathcal{C}_M)$. Here, M is the number of the elements. The element is usually the position of the "atoms" in the imaginary-time and/or real space. Although we can add three or many body interactions to obtain good efficiency of the SLMC, there is no systematic procedure to make good effective Hamiltonian.

In the field of MD, the machine learning and neural networks have been used for about twenty years to construct effective inter-atom or inter-molecule potentials to fit the PESs calculated by the first-principle calculations. We point out that the BPNNs can be considered as a general scheme to construct effective Hamiltonians. We show the method to reproduce the effective Hamiltonian with many-body interactions as follows.

IV. MACHINE LEARNING TECHNIQUE IN MOLECULAR DYNAMICS: BEHLER-PARRINELLO NEURAL NETWORKS

Machine learning techniques are widely used in the research fields of physics and chemistry. For example, "material informatics" has been developing rapidly³¹. Another remarkable development can be found in MD simulations. Machine learning techniques enable us to perform MD simulations in large systems with high accuracy comparable to quantum mechanical calculation (e.g., density functional theory) and low computational costs close to classical MD. We briefly introduce the machine learning techniques in MD simulations in this section.

A. Potential energy surfaces

The basic procedure to realize large-system MD simulation is construction of PESs in the large systems by "patching" PESs obtained in the small systems. The outline is shown below. First, we prepare a small system consisting of $N^{(s)}$ atoms. Quantum mechanical calculations are performed to obtain an accurate PES $E_{\text{tot}}^{(s)}(\mathcal{R}^{(s)})$, where $\mathcal{R}^{(s)} = \{\mathbf{r}_i | i = 1, \dots, N^{(s)}\}$ and \mathbf{r}_i are a set representing an atom configuration and the coordinate of the i -th atom, respectively.

Next, the total energy in the small system $E_{\text{tot}}^{(s)}(\mathcal{R}^{(s)})$ is assumed to be divided into "partial energies" associated with each atoms in the system, which are determined by "environment" around each atoms, i.e.,

$$E_{\text{tot}}^{(s)}(\mathcal{R}^{(s)}) = \sum_{i=1}^{N^{(s)}} E_{\text{part}}^{(s)}(\Delta_i^{(s)}), \quad (18)$$

where

$$\Delta_i^{(s)} = \{\mathbf{r}_{ij} | j = 1, \dots, i-1, i+1, \dots, N^{(s)}\} \quad (19)$$

is a set representing an atom configuration around the i -th atom ($\mathbf{r}_{ij} = \mathbf{r}_j - \mathbf{r}_i$).

B. Symmetry and descriptor

Here, we consider energy degeneracy due to translational and rotational invariance of the energy, i.e., energies given by a configuration and translated and rotated ones have a same value. Elimination of the degeneracy is desired for accurate evaluation of PES. Therefore, a set called "descriptor" (or "fingerprint")³¹ is introduced as

$$\mathcal{F}_i^{(s)} = \{F_I(\Delta_i^{(s)}) | I = 1, \dots, M\}, \quad (20)$$

where F_I and M are a function $F_I : \Delta_i^{(s)} \rightarrow \mathbb{R}$ and the number of them, respectively. Using the descriptor, the

total energy is given as

$$E_{\text{tot}}^{(S)}(\mathcal{R}^{(S)}) = \sum_{i=1}^{N^{(S)}} E_{\text{part}}^{(S)}(\mathcal{F}_i^{(S)}) , \quad (21)$$

The descriptor $\mathcal{F}_i^{(S)}$ is typically a set of functions of relative distances between atoms and angles between two vectors from one atom to other two atoms, which are obviously translational and rotational invariant. For example, the following function was proposed^{44,45},

$$F_I^{(d)}(\Delta_i^{(S)}) = \sum_{j=1, j \neq i}^{N^{(S)}} f_{i,j;I}^{(d)} , \quad (22)$$

$$f_{i,j;I}^{(d)} = \exp \left[-\eta_I (r_{ij} - r_I)^2 \right] , \quad (23)$$

where $r_{ij} = |\mathbf{r}_{ij}|$ and η_I and r_I are parameters. The function (23) works as a detector of bond length around r_I , and it is obviously translational and rotational invariant. Here is another example of the function^{44,45},

$$F_I^{(a)}(\Delta_i^{(S)}) = \sum_{j=1, j \neq i}^{N^{(S)}} \sum_{k=1, k \neq i, j}^{N^{(S)}} f_{i,j,k;I}^{(a)} , \quad (24)$$

$$f_{i,j,k;I}^{(a)} = 2^{1-\zeta_I} (1 + \lambda_I \cos \theta_{ijk})^{\zeta_I} e^{-\eta_I (r_{ij} + r_{ik})} , \quad (25)$$

where $\theta_{ijk} = \mathbf{r}_{ij} \cdot \mathbf{r}_{ik} / r_{ij} r_{ik}$ and ζ_I and λ_I are parameters. This function can detect the angle, and it is also translational and rotational invariant. These functions are usually used as elements of a descriptor, i.e.,

$$F_I = \begin{cases} F_I^{(d)} & (I = 1, \dots, m) \\ F_I^{(a)} & (I = m + 1, \dots, M) \end{cases} . \quad (26)$$

C. Extension from small systems to large systems

Toward the extension from small systems to large systems, we introduce a further assumption: the partial energy $E_{\text{part}}^{(S)}(\mathcal{F}_i^{(S)})$ can be approximately determined by the configuration of the atoms whose distances from the i -th atom are less than a cutoff radius r_c . It is realized by introducing a new descriptor

$$\mathcal{G}_i^{(S)}(r_c) = \left\{ G_I(\Delta_i^{(S)}; r_c) \mid I = 1, \dots, M \right\} , \quad (27)$$

where the function G_I satisfies the following condition:

$$G_I(\tilde{\Delta}_i^{(S)}; r_c) = 0 , \quad (28)$$

$$\begin{aligned} & \tilde{\Delta}_i^{(S)}(r_c) \\ &= \left\{ \mathbf{r}_{ij} \mid r_{ij} > r_c, j = 1, \dots, i-1, i+1, \dots, N^{(S)} \right\} . \end{aligned} \quad (29)$$

Using the functions, we obtain the following equation.

$$E_{\text{part}}^{(S)}(\mathcal{F}_i^{(S)}) \simeq E_{\text{part}}^{(S)}(\mathcal{G}_i^{(S)}(r_c)) , \quad (30)$$

This assumption means that the partial energies are determined by not global configurations $\Delta_i^{(S)}$ but local ones $\Delta_i^{(S)} \setminus \tilde{\Delta}_i^{(S)}(r_c) = \{\mathbf{r}_{ij} \mid r_{ij} \leq r_c, j = 1, \dots, i-1, i+1, \dots, N^{(S)}\}$. Note that the assumption is justified when there is no long range interaction among the atoms or long range interactions are screened in a system. We show an example of functions for the local descriptor below,

$$G_I = \begin{cases} G_I^{(d)} & (I = 1, \dots, m) \\ G_I^{(a)} & (I = m + 1, \dots, M) \end{cases} , \quad (31)$$

$$G_I^{(d)}(\Delta_i^{(S)}; r_c) = \sum_{j=1, j \neq i}^{N^{(S)}} f_{i,j;I}^{(d)} \xi_{ij}(r_c) , \quad (32)$$

$$G_I^{(a)}(\Delta_i^{(S)}; r_c) = \sum_{j,k=1, j,k \neq i, k \neq j}^{N^{(S)}} f_{i,j,k;I}^{(a)} \xi_{ij}(r_c) \xi_{ik}(r_c) , \quad (33)$$

$$\xi_{ij}(r_c) = \begin{cases} \frac{1}{2} \left[\cos \left(\frac{\pi r_{ij}}{r_c} \right) + 1 \right] & (r_{ij} \leq r_c) \\ 0 & (r_{ij} > r_c) \end{cases} . \quad (34)$$

Finally, we obtain the following partitioning of the total energy to the partial energies,

$$E_{\text{tot}}^{(S)}(\mathcal{R}^{(S)}) = \sum_{i=1}^{N^{(S)}} E_{\text{part}}^{(S)}(\mathcal{G}_i^{(S)}(r_c)) , \quad (35)$$

This partitioning enables us to extend MD simulations from the small system to a large system by constructing the total energy in the large system $E_{\text{tot}}^{(L)}$ as

$$E_{\text{tot}}^{(L)}(\mathcal{R}^{(L)}) = \sum_{i=1}^{N^{(L)}} E_{\text{part}}^{(S)}(\mathcal{G}_i^{(L)}(r_c)) , \quad (36)$$

where

$$\mathcal{R}^{(L)} = \left\{ \mathbf{r}_i \mid i = 1, \dots, N^{(L)} \right\} , \quad (37)$$

$$\mathcal{G}_i^{(L)}(r_c) = \left\{ G_I(\Delta_i^{(L)}; r_c) \mid I = 1, \dots, M \right\} , \quad (38)$$

$$\Delta_i^{(L)} = \left\{ \mathbf{r}_{ij} \mid j = 1, \dots, i-1, i+1, \dots, N^{(L)} \right\} , \quad (39)$$

and $N^{(L)}$ is the number of atoms in the large system. We mention that the function $E_{\text{part}}^{(S)}$ defined in the small system works even with the local descriptor in the large system $\mathcal{G}_i^{(L)}(r_c)$. Because it contains information of the atom configuration within the cutoff r_c , which is consistent with the local descriptor in the small system.

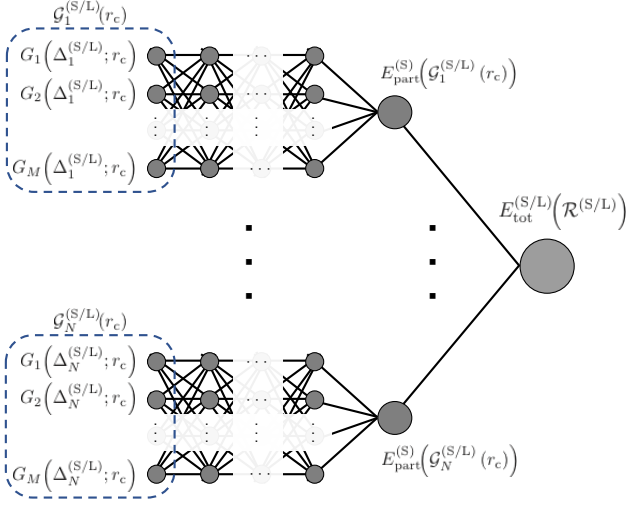


FIG. 2. Schematics of the Behler-Parrinello high-dimensional neural networks. This figure shows an example corresponding to a system containing N atoms and M descriptor functions.

D. Behler–Parrinello neural networks

Now we have a method of the extension. The remaining problem is how to obtain the function $E_{\text{part}}^{(S)}$. Machine learning techniques give a solution of the problem. Behler and Parrinello (BP) proposed an energy partitioning method using neural networks (NNs)⁴⁴, i.e., the partial energies are determined by HDNNS. Figure 2 shows a schematics of the BP-NN method. Although this approach loses explicit physical meaning of the partial energies, it is effective. It is a common issue about application of machine learning techniques, i.e., machine learning works as a black box.

We mention that there was a serious problem about the descriptors. The number of the descriptors blows up as increase of the number of atom types. For example, the number of descriptors is in proportion to $N_t C_3$ if they contain the angles between the centered atom and other two atoms when they have N_t types. Artrith *et al.* solved the problem by introducing new descriptor using the Chebyshev polynomials⁴⁶. The new descriptor expresses information of the radial and angular distribution functions including information of the atom types by Chebyshev coefficients. They were succeeded in providing accurate energies of materials containing eleven atom types⁴⁶.

E. Similarity between first-principle-based MD and QMC

Before closing this section, let us discuss the similarity between first-principle-based MD and QMC, as shown in Table.II. In first-principle-based MD simulations, forces

among atoms are needed for the dynamics, which are obtained by derivative of the total energy, i.e., the total energy as a function of the atom configuration is the essential quantity. On the other hand, in QMC simulations, the Monte Carlo weights are critical quantity, which is also a function of the configuration. These two methods are not similar on the view point of algorithm and physical meaning. But there is a similarity: both of the energies in MD and Monte carlo weights are functions of the configuration. Therefore, we can apply the machine learning techniques in MD simulations to speedup the QMC simulations based on the similarity.

V. COMBINE SLMC WITH BPNN

A. General Effective Hamiltonian in SLMC

As described in the previous section, the total energy in the BP neural network is expressed by the sum of the “partial” energies associated with each atoms in the system. This expression enables us to have a portability: one can increase the number atoms with same neural networks. According to this method, we introduce the effective Hamiltonian expressed as the sum of the “element-wise” Hamiltonian:

$$H_{\text{eff}}(\mathcal{C}) = \sum_{j=1}^N h_{\text{eff}}^{\alpha_j}(N, \mathcal{C}^j), \quad (40)$$

where \mathcal{C}^j is an “element-wise” configuration around an “atom” j , which corresponds to Eq. (19) in the original BP method. Here, N is a number of atoms and α_j is a kind of atoms. The above division is justified in Fermion systems as follows.

In fermion systems, most methods in various kinds of systems calculate the partition function Z expressed as the determinant of the matrix:

$$Z = \sum_{\mathcal{C}} \det M(\mathcal{C}) = \sum_{\mathcal{C}} w(\mathcal{C}). \quad (41)$$

The dimension of the matrix depends on a method. For example, in continuous-time QMC (e.g. CT-AUX and CT-INT) for an impurity model, the dimension of the matrix M is the number of the vertices on the imaginary-time axis. The logarithm of the original weight can be expressed as the sum of the “element-wise” Hamiltonian, since the logarithm of the weight $\ln w(\mathcal{C})$ is expressed as

$$\ln w(\mathcal{C}) = \ln \det M(\mathcal{C}), \quad (42)$$

$$= \sum_{j=1}^N [\ln M(\mathcal{C})]_{jj}. \quad (43)$$

Therefore, the effective Hamiltonian defined in Eq. (40) can imitate the original model.

B. Effective Hamiltonian in SLMC

In actual SLMC simulations, we adopt the effective Hamiltonian defined as

$$H_{\text{eff}}(\mathcal{C}) = \frac{1}{N} \sum_{j=1}^N h_{\text{eff}}^{\alpha_j}(\mathbf{c}^j) + f(N), \quad (44)$$

Here, $f(N)$ is a polynomial function $f(N) = \sum_{k=0}^{n_{\text{max}}} f_k N^k$. We assume $t h_{\text{eff}}^{\alpha_j}(N, \mathbf{c}^j) = (1/N) h_{\text{eff}}^{\alpha_j}(\mathbf{c}^j)$. This factor $1/N$ is introduced as the normalization, which is appropriate for the CTAUX in the previous paper. The $h_{\text{eff}}^{\alpha_j}(\mathbf{c}^j)$ is constructed by neural networks. Note that the nonlinear function $h_{\text{eff}}^{\alpha_j}(\mathbf{c}^j)$ does not depend on j and only depends on α_j , since we assume that the same kind of atoms feels same interactions.

C. Construction of the element-wise configurations

We have to generate element-wise configurations \mathbf{c}^j from \mathcal{C} . Usually, in QMC simulations, the configuration \mathcal{C} is a set of positions of "atoms" (e.g. spins or vertices) on real and/or imaginary-time axes. We can make the element-wise configurations \mathbf{c}^j which consist of the distances between the atom j and other atoms. However, if a coordinate is continuous, the set of distances is not a good configuration since the number of elements of the input vector \mathbf{c}^j depends on the number of atoms: we can not increase the number of atoms. In continuous-time QMC simulations, the number of atoms changes during simulations.

One of the method to construct the element-wise configurations on continuous axis is the Chebyshev polynomial expansion method in the field of machine-learning MD simulations⁴⁶. The element-wise configuration is expressed by the basis functions as follows. For simplicity, we consider a configuration which has vertices on the imaginary-time axis such as a quantum impurity model. We map the configuration \mathcal{C} onto the set of the element-wise configurations $\mathcal{C}^{\text{ele}}(\tau_i - \tau_j)$ around a vertex j : $\mathcal{C} \rightarrow \{\mathcal{C}^{\text{ele}}(\tau_1 - \tau_j), \mathcal{C}^{\text{ele}}(\tau_2 - \tau_j), \dots, \mathcal{C}^{\text{ele}}(\tau_N - \tau_j)\}$. The element-wise configuration is expressed by the basis functions. We introduce the density distribution functions defined as

$$\rho(\tau, \mathcal{C}^{\text{ele}}(\tau_i - \tau_j)) = \sum_{i=1}^N \delta(\tau - \tau_{ij}), \quad (45)$$

where $\tau_{ij} = 2|\tau_i - \tau_j|/\beta - 1$ is the distance between atom i and atom j . This distribution is expanded by the Chebyshev polynomial functions⁴⁶:

$$\rho(\tau, \mathcal{C}^{\text{ele}}(\tau_i - \tau_j)) = \sum_m c_m^j \phi_m(\tau), \quad (46)$$

where

$$c_m^j = \sum_{i=1}^N \phi_m(\tau_{ij}). \quad (47)$$

Here, $\phi_m(x)$ is the Chebyshev polynomial function $\phi_m(x) = \cos(m \arccos(x))$. Thus, we map the element-wise configuration $\mathcal{C}^{\text{ele}}(\tau_i - \tau_j)$ onto the set of m_{cut} coefficients of the Chebyshev polynomials $\mathcal{C}^{\text{ele}}(\tau_i - \tau_j) \rightarrow \{c_0^j, \dots, c_{m_{\text{cut}}-1}^j\}$, as shown in Fig. 1. The element-wise configuration \mathbf{c}^j is expressed as $\mathbf{c}^j \equiv \{c_0^j, \dots, c_{m_{\text{cut}}-1}^j\}$, which does not depend on the number of atoms.

To introduce a difference of species, we can add another distribution functions. For example, if the vertex has a spin index s_j and there is spin-reversal symmetry (i.e. the weight is not changed by flipping all spins), it is better to add "spin-density" distribution functions defined as

$$\rho_s(\tau, \mathcal{C}^{\text{ele}}(\tau_i - \tau_j)) = \sum_{i=1}^N s_i s_j \delta(\tau - \tau_{ij}), \quad (48)$$

With the use of the Chebyshev polynomial expansions, we have

$$\rho_s(\tau, \mathcal{C}^{\text{ele}}(\tau_i - \tau_j)) = \sum_m d_m^j \phi_m(\tau), \quad (49)$$

where

$$d_m^j = \sum_{i=1}^N s_i s_j \phi_m(\tau_{ij}). \quad (50)$$

Then, the element-wise configuration \mathbf{c}^j is $\mathbf{c}^j \equiv \{c_0^j, \dots, c_{m_{\text{cut}}-1}^j, d_0^j, \dots, d_{m_{\text{cut}}-1}^j\}$.

D. Relation between the SLMC with BPNN and previous effective model

In the previous paper in the CTAUX QMC, the configuration \mathcal{C} consists of vertices with a spin index on the imaginary-time continuous axis. We show that the effective Hamiltonian in this previous paper can be regarded as Eq. (44) with linear functions $h_{\text{eff}}^{\alpha_j}(\mathbf{c}^j)$ without hidden layers. If the function $h_{\text{eff}}^{\alpha_j}(\mathbf{c}^j)$ is linear, the effective Hamiltonian is expressed as

$$H_{\text{eff}}(\mathcal{C}) = \frac{1}{N} \sum_{j=1}^N W^T \mathbf{c}^j + b + f(N). \quad (51)$$

Here, W is M -dimensional vector and M is the number of the input elements. With the use of the element-wise configuration \mathbf{c}^j is $\mathbf{c}^j \equiv \{c_0^j, \dots, c_{m_{\text{cut}}-1}^j, d_0^j, \dots, d_{m_{\text{cut}}-1}^j\}$, this effective Hamiltonian is rewritten as

$$H_{\text{eff}}(\mathcal{C}) = \frac{1}{N} \sum_{j=1}^N \sum_{m=1}^{m_{\text{cut}}} W_l^c c_{l-1}^j + \frac{1}{N} \sum_{j=1}^N \sum_{m=1}^{m_{\text{cut}}} W_l^d d_{l-1}^j + f(N). \quad (52)$$

Here, the coefficient b is included in $f(N)$. With the use of Eqs. (47) and (50), we obtain

$$H_{\text{eff}}(\mathcal{C}) = \frac{1}{N} \sum_{i,j=1}^N L(\tau_i - \tau_j) + \frac{1}{N} \sum_{i,j=1}^N J(\tau_i - \tau_j) s_i s_j + f(N), \quad (53)$$

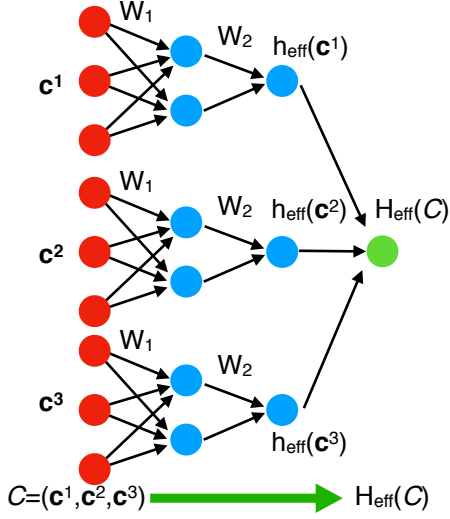


FIG. 3. (Color online) Schematic figures of input and output data in Behler-Parrinello neural networks. The weight is expressed as a sum of the element-wise effective Hamiltonians. If we neglect hidden layers, the effective Hamiltonian is constructed by linear combinations.

where

$$L(\tau_i - \tau_j) \equiv \sum_{m=1}^{m_{\text{cut}}} W_l^c \phi_m(\tau_{ij}), \quad (54)$$

$$J(\tau_i - \tau_j) \equiv \sum_{m=1}^{m_{\text{cut}}} W_l^d \phi_m(\tau_{ij}). \quad (55)$$

This effective Hamiltonian is completely equivalent to that used in the previous paper.

E. Many body interactions with neural networks

The effective Hamiltonian with linear functions $h_{\text{eff}}^{\alpha_j}(\mathbf{c}^j)$ includes only two-body interactions as shown in Eq. (53). To include the many-body interactions, we can add hidden layers. For example, in the case of the neural networks with one hidden layer with N_u units, the effective element-wise Hamiltonian is expressed as

$$h_{\text{eff}}^{\alpha_j}(\mathbf{c}^j) = \hat{W}_2^{\alpha_j} F(\hat{W}_1^{\alpha_j} \mathbf{c}^j + \mathbf{b}_1^{\alpha_j}) + b_2^{\alpha_j}, \quad (56)$$

with the activation function $[F(\mathbf{x})]_i = F([\mathbf{x}]_i)$. Here, $\hat{W}_1^{\alpha_j}$ is the $N_u \times M$ matrix, $\hat{W}_2^{\alpha_j}$ is $1 \times N_u$ matrix, $\mathbf{b}_1^{\alpha_j}$ is the N_u -dimensional bias vector, and $b_2^{\alpha_j}$ is the bias. The activation function $F(x)$ makes the effective Hamiltonian nonlinear, which can represent many-body interactions. The schematic figure of the effective Hamiltonian is shown in Fig. 3. We use same weight matrix W with same atomic species.

VI. DEMONSTRATIONS ON QUANTUM IMPURITY MODELS

A. Continuous-time QMC for fermions

In continuous-time QMC simulations, by splitting the Hamiltonian into non-perturbative and perturbative parts $H = H_0 + H_1$, the partition function is expanded as

$$Z = \text{Tr} \left[e^{-\beta H_0} T_\tau e^{-\int_0^\beta H_1(\tau) d\tau} \right], \quad (57)$$

$$= \sum_{N=0}^{\infty} \frac{(-1)^N}{N!} \int_0^\beta d\tau_1 \cdots \int_0^\beta d\tau_N \text{Tr} [T_\tau e^{-\beta H_0} H_1(\tau_N) \times H_1(\tau_{N-1}) \cdots H_1(\tau_1)], \quad (58)$$

$$= \sum_{\mathcal{C}} W(\mathcal{C}). \quad (59)$$

Here, a configuration \mathcal{C} has N vertices on the imaginary-time axis¹³. The number of vertices N changes during simulation.

B. Continuous-Time interaction expansion quantum Monte Carlo in impurity models

We demonstrate self-learning CTINT with BPNNs on impurity model. The CTINT method is a good example to demonstrate the SLMC with BPNN, since Huang *et al.* claimed that the three body interactions are needed to construct good effective model in CTINT method.²¹

We consider the Hamiltonian of the single impurity Anderson model, which is written as the combination of a free fermion part and interaction part^{13,22},

$$H = -\mu \sum_{\sigma} n_{\sigma} + \sum_{\sigma,p} (V c_{\sigma}^{\dagger} a_{p,\sigma} + \text{H.c.}) + \sum_{\sigma,p} \epsilon_p a_{p,\sigma}^{\dagger} a_{p,\sigma} + U n_{\uparrow} n_{\downarrow}, \quad (60)$$

where $\sigma = \uparrow, \downarrow$, c_{σ}^{\dagger} and $a_{p,\sigma}^{\dagger}$ are the fermion creation operators for an impurity electron with spin σ , and that for a bath electron with spin σ and momentum p , respectively. n_{σ} is the impurity electron number operator. We consider a bath with a semicircular density of states $\rho_0(\epsilon) = [2/(\pi D) \sqrt{1 - (\epsilon/D)^2}]$ and set the half bandwidth $D = 1$ as the energy unit. In the CTINT algorithm, we rewrite the interaction part expressed as

$$H_1 = \frac{U}{2} \sum_{s=\pm 1} \left(n_{\uparrow} - \frac{\rho}{2} - s\delta \right) \left(n_{\downarrow} - \frac{\rho}{2} + s\delta \right). \quad (61)$$

Here, we introduce additional Ising variable s and parameter δ , and ρ corresponds to the average electron density⁵¹⁻⁵³. We consider the half filling ($\rho = 1$). The non-perturbative part is $H_0 = (-\mu + \frac{U}{2} \rho) \sum_{\sigma} n_{\sigma} +$

$\sum_{\sigma,p}(Vc_{\sigma}^{\dagger}a_{p,\sigma} + \text{H.c.}) + \sum_{\sigma,p}\epsilon_p a_{p,\sigma}^{\dagger}a_{p,\sigma}$. The partition function is expanded as

$$\frac{Z}{Z_0} = \sum_{\mathcal{C}} W(\mathcal{C}) = \sum_{\mathcal{C}} \left(\frac{-U}{2} \right)^N \frac{1}{N!} \prod_{\sigma} \det M_{\sigma}(\mathcal{C}). \quad (62)$$

Here, the $N \times N$ matrix $M_{\sigma}(\mathcal{C})$ is defined by $[M_{\sigma}(\mathcal{C})]_{ij} \equiv g_0(\tau_i - \tau_j) - \alpha_{\sigma}(s_n)\delta_{ij}$ with $\alpha_{\sigma}(s) \equiv \rho/2 + \sigma s\delta$. $g_0(\tau_i - \tau_j)$ is the free fermion Green's function at the impurity site. We implement the CTINT with the Julia language 0.6.2 and gather training data in this code. We train the neural networks with one hidden layer as shown in Fig. 3 with 50000 training data, which is done by the TensorFlow 1.4, one of the deep learning frameworks, in Python 3.6.5. The sigmoid function $F(x) = 1/(1 + \exp(-x))$ is used as the activation function. We develop the batch-atom normalization, variant of the batch normalization⁵⁴ which is one of the modern techniques accelerating training procedures for neural network by normalizing along batch index. In the batch-atom normalization, we normalize both batch and atomic index j (See, Appendix A). The input vector is $M = 2m_{\text{cut}}$ dimensional vector: $\mathbf{c}^j = (c_{0,0}^j, \dots, c_{m_{\text{cut}}-1,0}^j, d_{0,0}^j, \dots, d_{m_{\text{cut}}-1,0}^j)^T$. The total number of parameters in neural networks with one hidden layer with N_u units is $MN_u + N_u + 4N_u + N_u + n_{\text{max}} + 1 = MN_u + 6N_u + n_{\text{max}} + 1$.

Figure 4 shows the inverse-temperature dependence of the acceptance ratio of the SLMC. We consider $U = 3D$, $\delta = 0.5$, $V = 1D$, and $n_{\text{max}} = 3$. We set the number of the SLMC steps n is $n = 500$. We also consider the linear SLMC, which is equivalent to the previous effective Hamiltonian²². In the case with $\beta = 40$, the acceptance ratio with 10 units ($N_u = 10$) is around 0.8, while that of the linear SLMC is less than 0.02. The results indicate that the BPNNs can systematically improve the effective Hamiltonian with increasing the number of units.

VII. DISCUSSION

A. Computational cost and fast updates.

We estimate the computational cost of SLMC with BPNNs. The computational cost to calculate the element-wise effective Hamiltonian $h_{\text{eff}}(\mathbf{c}^j)$ with the neural networks with one hidden layer is $\mathcal{O}(N_u M)$ when the M -dimensional input vector \mathbf{c}^j are given. The computational cost to calculate the coefficients \mathbf{c}^j is $\mathcal{O}(N)$ since there are N δ -functions shown in Eq. (46). Thus, the computational cost to calculate the effective Hamiltonian $H_{\text{eff}}(\mathcal{C})$ is $\mathcal{O}(N_u M N^2)$, whose order is equivalent to that in the original CTINT simulation with fast updates^{13,22}. To speedup SLMC, we reduce the cost to calculate the coefficients $\mathcal{O}(N)$ to $\mathcal{O}(1)$ with fast local updates. If we consider the insertion of the vertex, the new coefficient $c_m^{j,\text{new}}$ is calculated as $c_m^{j,\text{new}} = c_m^{j,\text{old}} + \phi_m(\tau_{iN+1})$, whose calculation cost is $\mathcal{O}(1)$. With use of this local

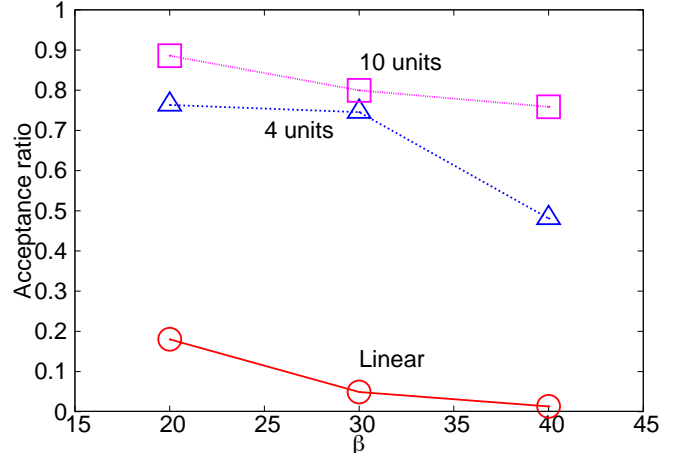


FIG. 4. (Color online) Inverse-temperature dependence of the acceptance ratio in the self-learning continuous-time interaction expansion quantum Monte Carlo simulation in the Anderson impurity model. We consider $U = 3D$, $\delta = 0.5$, $V = 1D$ and 500 SLMC steps.

update, the total computational cost to calculate the effective Hamiltonian is $\mathcal{O}(N_u M N)$. Therefore, the order of the computational cost of SLMC with BPNNs as a functional of N is equivalent to that in SLMC in the previous paper for the CTAUX²².

VIII. CONCLUSION

We developed SLMC method with BPNNs, which can be considered as a general scheme to construct effective Hamiltonians with many body interactions even on continuous axis. We demonstrated the continuous-time interaction-expansion (CTINT) SLMC with BPNNs on quantum impurity models. The effective Hamiltonian without any prior knowledge was obtained. We obtained the significant improvement of the acceptance rate with respect to the SLMC with the effective Hamiltonian using explicit expression. This improvement implies that obtained effective Hamiltonian of SLMC with BPNNs includes many body interaction effects, which is omitted in the effective Hamiltonians with the explicit forms. Our SLMC with BPNNs has many potential applications, since this method can accept both continuous and discrete indices of interacting particles as inputs of neural networks.

ACKNOWLEDGEMENT

Y. N. would like to acknowledge H. Shen, Y. Qi and L. Fu for helpful discussions and comments. The calculations were partially performed by the supercomputing systems SGI ICE X at the Japan Atomic Energy Agency.

This work was partially supported by JSPS–KAKENHI Grant Numbers 18K03552 to Y.N. and 18K05208 to M.O. and the “Topological Materials Science” (No. 18H04228) JSPS–KAKENHI on Innovative Areas to Y.N..

Appendix A: Batch-atom normalization

We describe the detail of the batch-atom normalization in the CTINT QMC simulation. We consider neural networks with one hidden layer. The input vector is $\mathbf{c}^j = (c_0^j, \dots, c_{m_{cut}-1}^j, d_0^j, \dots, d_{m_{cut}-1}^j)^T$. Here, the coefficients are defined as

$$c_m^j = \sum_{i=1}^N \phi_m(\tau_{ij}), \quad (\text{A1})$$

$$d_m^j = \sum_{i=1}^N s_i s_j \phi_m(\tau_{ij}), \quad (\text{A2})$$

with the pseudo-spin index s_i . The effective Hamiltonian is defined as

$$H_{\text{eff}}(\mathcal{C}) = \frac{1}{N} \sum_{j=1}^N h_{\text{eff}}(\mathbf{c}^j) + f(N), \quad (\text{A3})$$

where

$$h_{\text{eff}}(\mathbf{c}^j) = \hat{W}_2 F(\hat{W}_1 \mathbf{c}^j + \mathbf{b}_1) + b_2, \quad (\text{A4})$$

$$= \sum_{j_1=1}^{N_u} [\hat{W}_2]_{j_1} F([\mathbf{x}]_{j_1}^j) + b_2, \quad (\text{A5})$$

where

$$[\mathbf{x}]_{j_1}^j \equiv \sum_{j_2=1}^M [\hat{W}_1]_{j_1 j_2} [\mathbf{c}^j]_{j_2} + [\mathbf{b}_1]_{j_1} \quad (\text{A6})$$

Here, $[F(\mathbf{x})]_i = F([\mathbf{x}]_i)$ denotes the activation function, \hat{W}_1 is the $N_u \times M$ matrix, \hat{W}_2 is $1 \times N_u$ matrix, \mathbf{b}_1 is the N_u -dimensional bias vector, b_2 is the bias, and M is a number of coefficients \mathbf{c}^j . We introduce the batch-atom normalization function G as

$$h_{\text{eff}}(\mathbf{c}^j) = \sum_{j_1=1}^{N_u} [\hat{W}_2]_{j_1} G(F([\mathbf{x}]_{j_1}^j)) + b_2, \quad (\text{A7})$$

where

$$G(F([\mathbf{x}]_{j_1}^j)) = \gamma_{j_1} \frac{F([\mathbf{x}]_{j_1}^j) - \mu_{j_1}}{\sqrt{\sigma_{j_1}^2 + \epsilon^2}} + \beta_{j_1}. \quad (\text{A8})$$

Here, the parameters γ_{j_1} and β_{j_1} are trainable parameters. ϵ is a small number. The batch-atom mean μ_{j_1} and variance σ_{j_1} are defined as

$$\mu_{j_1} = \frac{1}{N N_{\text{batch}}} \sum_{l=1}^{N_{\text{batch}}} \sum_{j=1}^N F([\mathbf{x}]_{j_1}^l), \quad (\text{A9})$$

$$\sigma_{j_1}^2 = \frac{1}{N N_{\text{batch}}} \sum_{l=1}^{N_{\text{batch}}} \sum_{j=1}^N \left(F([\mathbf{x}]_{j_1}^l) - \mu_{j_1} \right)^2. \quad (\text{A10})$$

The index l in \mathbf{x}^l is the index of the training data. Here, N_{batch} is the number of the batch size of the training data.

-
- ¹ R. H. Swendsen and J.-S. Wang, Phys. Rev. Lett. **58**, 86 (1987).
² U. Wolff, Phys. Rev. Lett. **62**, 361 (1989).
³ N. Prokof'ev, B. Svistunov, and I. Tupitsyn, Phys. Lett. A **238**, 253 (1998).
⁴ H. G. Evertz, G. Iana, and M. Marcu, Phys. Rev. Lett. **70**, 875 (1993).
⁵ H. G. Evertz, Adv. Phys. **52**, 1 (2003).
⁶ S. Beyl, F. Goth, and F. F. Assaad, Revisiting the hybrid quantum Monte Carlo method for Hubbard and electron-phonon models, Phys. Rev. B **97**, 085144 (2018).
⁷ R. Blankenbecler, D. J. Scalapino, and R. L. Sugar, Monte Carlo calculations of coupled boson-fermion systems. I, Phys. Rev. D **24**, 2278 (1981).
⁸ J. E. Hirsch, Two-dimensional Hubbard model: Numerical simulation study, Phys. Rev. B **31**, 4403 (1985).
⁹ J. E. Hirsch and R. M. Fye, Monte Carlo Method for Magnetic Impurities in Metals, Phys. Rev. Lett. **56**, 2521

- (1986).
¹⁰ S. R. White, D. J. Scalapino, R. L. Sugar, E. Y. Loh, J. E. Gubernatis, and R. T. Scalettar, Numerical study of the two dimensional Hubbard model, Phys. Rev. B **40**, 506 (1989).
¹¹ A. N. Rubtsov, V. V. Savkin, and A. I. Lichtenstein, Continuous time quantum Monte Carlo method for fermions, Phys. Rev. B **72**, 035122 (2005).
¹² P. Werner, A. Comanac, L. de Medici, M. Troyer, and A. J. Millis, Continuous-Time Solver for Quantum Impurity Models, Phys. Rev. Lett. **97**, 076405 (2006).
¹³ E. Gull, A. J. Millis, A. I. Lichtenstein, A. N. Rubtsov, M. Troyer, and P. Werner, Continuous-time Monte Carlo methods for quantum impurity models, Rev. Mod. Phys. **83**, 349 (2011).
¹⁴ E. Gull, P. Werner, O. Parcollet and M. Troyer, Continuous-time auxiliary-field Monte Carlo for quantum impurity models, Europhys. Lett. **82**, 57003 (2008).

- ¹⁵ J. Liu, Y. Qi, Z. Y. Meng, and L. Fu, Self-learning Monte Carlo method, *Phys. Rev. B* **95**, 041101(R) (2017).
- ¹⁶ L. Huang and L. Wang, Accelerated Monte Carlo simulations with restricted Boltzmann machines, *Phys. Rev. B* **95**, 035105 (2017).
- ¹⁷ J. Liu, H. Shen, Y. Qi, Z. Y. Meng, and L. Fu, Self-learning Monte Carlo method and cumulative update in fermion systems, *Phys. Rev. B* **95**, 241104(R) (2017).
- ¹⁸ X. Y. Xu, Y. Qi, J. Liu, L. Fu, and Z. Y. Meng, Self-learning quantum Monte Carlo method in interacting fermion systems, *Phys. Rev. B* **96**, 041119(R).
- ¹⁹ Z. H. Liu, X. Y. Xu, Y. Qi, K. Sun, Z. Y. Meng, Itinerant quantum critical point with frustration and non-Fermi-liquid, arXiv:1706.10004
- ²⁰ C. Chen, X. Y. Xu, J. Liu, G. Batrouni, R. Scalettar, and Z. Y. Meng, Symmetry-enforced self-learning Monte Carlo method applied to the Holstein model, *Phys. Rev. B* **98**, 041102(R) (2018).
- ²¹ L. Huang, Y.-f. Yang, and L. Wang, Recommender engine for continuous-time quantum Monte Carlo methods, *Phys. Rev. E* **95**, 031301(R) (2017).
- ²² Y. Nagai, H. Shen, Y. Qi, J. Liu, and L. Fu, Self-learning Monte Carlo method: Continuous-time algorithm, *Phys. Rev. B* **96**, 161102(R) (2017).
- ²³ A. Tanaka and A. Tomiya, Towards reduction of autocorrelation in HMC by machine learning, arXiv:1712.03893
- ²⁴ L. Zdeborova, Machine learning: New tool in the box, *Nat. Phys.* **13**, 420 (2017).
- ²⁵ J. Carrasquilla and R. G. Melko, Machine learning phases of matter, *Nat. Phys.* **13**, 431 (2017).
- ²⁶ G. Carleo and M. Troyer, Solving the quantum many-body problem with artificial neural networks, *Science* **355**, 602 (2017).
- ²⁷ A. Tanaka and A. Tomiya, Detection of Phase Transition via Convolutional Neural Networks, *J. Phys. Soc. Jpn.* **86**, 063001 (2017).
- ²⁸ E. P. L. van Nieuwenburg, Y.-H. Liu, and Sebastian D. Huber, Learning phase transitions by confusion, *Nat. Phys.* **13**, 435 (2017).
- ²⁹ Yi Zhang, and E.-A. Kim, Quantum Loop Topography for Machine Learning, *Phys. Rev. Lett.* **118**, 216401 (2017).
- ³⁰ J. Chen, S. Cheng, H. Xie, L. Wang, and T. Xiang, Equivalence of restricted Boltzmann machines and tensor network states, *Phys. Rev. B* **97**, 085104 (2018).
- ³¹ R. Ramprasad, R. Batra, G. Pilania, A. Mannodi-Kanakkithodi, and C. Kim, Machine learning in materials informatics: recent applications and prospects, *npj Comp. Mater.* **3**, 54 (2017).aaa
- ³² D.-L. Deng, X. Li, and S. Das Sarma, Quantum Entanglement in Neural Network States, *Phys. Rev. X* **7**, 021021 (2017).
- ³³ Y. Huang, and J. E. Moore, Neural network representation of tensor network and chiral states, arXiv:1701.06246.
- ³⁴ W. Hu, R. R.P. Singh, R. T. Scalettar, Discovering Phases, Phase Transitions and Crossovers through Unsupervised Machine Learning: A critical examination, *Phys. Rev. E* **95**, 062122 (2017).
- ³⁵ Z. Cai, Approximating quantum many-body wavefunctions using artificial neural networks, *Phys. Rev. B* **97**, 035116 (2018).
- ³⁶ H. Fujita, Y. O. Nakagawa, S. Sugiura and M. Oshikawa, Construction of Hamiltonians by machine learning of energy and entanglement spectra, *Phys. Rev. B* **97**, 075114 (2018)
- ³⁷ S. J. Wetzel, and M. Scherzer, Machine Learning of Explicit Order Parameters: From the Ising Model to SU(2) Lattice Gauge Theory, *Phys. Rev. B* **96**, 184410 (2017).
- ³⁸ S. Iso, S. Shiba, S. Yokoo Scale-invariant Feature Extraction of Neural Network and Renormalization Group Flow, *Phys. Rev. E* **97**, 053304 (2018).
- ³⁹ T. Mano, and T. Ohtsuki Phase Diagrams of Three-Dimensional Anderson and Quantum Percolation Models Using Deep Three-Dimensional Convolutional Neural Network *J. Phys. Soc. Jpn.* **86**, 113704 (2017).
- ⁴⁰ H. Shen, J. Liu, and L. Fu, Self-learning Monte Carlo with deep neural networks *Phys. Rev. B* **97**, 205140 (2018).
- ⁴¹ T.B. Blank, S.D. Brown, A.W. Calhoun, and D.J. Doren, *J. Chem. Phys.* **103**, 4129 (1995).
- ⁴² D.F.R. Brown, Combining ab initio computations, neural networks, and diffusion Monte Carlo: An efficient method to treat weakly bound molecules, *J. Chem. Phys.* **105**, 7597 (1996).
- ⁴³ S. Lorenz, A. Groß, and M. Scheffler, Representing high-dimensional potential-energy surfaces for reactions at surfaces by neural networks, *Chem. Phys. Lett.* **395**, 210 (2004).
- ⁴⁴ J. Behler and M. Parrinello, Generalized Neural-Network Representation of High-Dimensional Potential-Energy Surfaces, *Phys. Rev. Lett.* **98**, 146401 (2007).
- ⁴⁵ J. Behler, Constructing High-Dimensional Neural Network Potentials: A Tutorial Review, *Int. J. Quantum Chem.* **115**, 1032 (2015).
- ⁴⁶ N. Artrith, A. Urban, and G. Ceder, Efficient and accurate machine-learning interpolation of atomic energies in compositions with many species, *Phys. Rev. B* **96**, 014112 (2017).
- ⁴⁷ N. Artrith, T. Morawietz, and J. Behler, High-dimensional neural-network potentials for multicomponent systems: Applications to zinc oxide, *Phys. Rev. B* **83**, 153101 (2011).
- ⁴⁸ N. Artrith and A.M. Kolpak, Understanding the Composition and Activity of Electrocatalytic Nanoalloys in Aqueous Solvents: A Combination of DFT and Accurate Neural Network Potentials, *Nano Lett.* **14**, 670 (2014).
- ⁴⁹ W. Li, Y. Ando, and S. Watanabe, Cu Diffusion in Amorphous Ta₂O₅ Studied with a Simplified Neural Network Potential, *J. Phys. Soc. Jpn.* **86**, 104004 (2017).
- ⁵⁰ W. Li and Y. Ando, Construction of accurate machine learning force fields for copper and silicon dioxide, arXiv:1807.02042.
- ⁵¹ F. F. Assaad and T. C. Lang, Diagrammatic determinantal quantum Monte Carlo methods: Projective schemes and applications to the Hubbard-Holstein model, *Phys. Rev. B* **76**, 035116 (2007).
- ⁵² F. F. Assaad, Continuous-time QMC Solvers for Electronic Systems in Fermionic and Bosonic Baths, in E. Pavarini, E. Koch, D. Vollhardt, and A. Lichtenstein (eds.), *DMFT at 25: Infinite Dimensions: Lecture Notes of the Autumn School on Correlated Electrons 4*, (Forschungszentrum Julich), ISBN 978-3-89336-953-9 (2014).
- ⁵³ D. J. Luitz and F. F. Assaad, Weak-coupling continuous-time quantum Monte Carlo study of the single impurity and periodic Anderson models with s-wave superconducting baths, *Phys. Rev. B* **81**, 024509 (2010).
- ⁵⁴ S. Ioffe and C. Szegedy, Batch normalization: Accelerating deep network training by reducing internal covariate shift, arXiv:1502.03167.
- ⁵⁵ The method how to treat many kinds of species in BP neural networks was proposed in Ref.⁴⁶.

⁵⁶ There is a relation between CTINT and CTAUX. The perturbation order becomes same when the parameter of the CTAUX has the relation: $K = U\beta(\delta^2 - 1/4)^{52}$.